PUBLISHED ONLINE: 6 JANUARY 2013
DOI: 10.1038/NPHOTON.2012.316

Experimental demonstration of a receiver beating the standard quantum limit for multiple nonorthogonal state discrimination

F. E. Becerra*,[1] J. Fan,[1] G. Baumgartner,[2] J. Goldhar,[3] J. T. Kosloski,[2] and A. Migdall[1]

[1]*Joint Quantum Institute, University of Maryland, and National Institute of Standards and Technology, 100 Bureau Drive, Gaithersburg, MD 20899*
[2]*Laboratory for Telecommunications Sciences, 8080 Greenmead Drive, College Park, MD 20740*
[3]*Department of Electrical and Computer Engineering, 2410 A.V. Williams Bldg., University of Maryland, College Park, MD 20742*

Measurement of the state of a quantum system with inherent quantum uncertainty (noise) approaching the ultimate physical limits is of both technological and fundamental interest. Quantum noise prevents any mutually nonorthogonal quantum states, such as coherent states, from being distinguished with perfect accuracy. Optimized quantum measurements for nonorthogonal coherent states allow in principle for state discrimination sensitivities surpassing the standard quantum limit (SQL). Realizing quantum receivers that can detect multiple coherent states with sensitivity levels approaching the ultimate quantum limits is fundamental to quantum-enhanced measurements, and can optimize the performance of quantum and classical communications as well as future implementations of quantum technologies. Here we demonstrate the first quantum receiver that unconditionally discriminates four nonorthogonal coherent states with error probabilities below the SQL. This receiver achieves error rates four times lower than is possible with any ideal conventional receiver with perfect detection efficiency.

Quantum mechanics sets fundamental limits on the attainable measurement uncertainty of mutually nonorthogonal states. Nonorthogonal coherent states cannot be distinguished with total certainty due to their intrinsic overlap[1]. Efficient measurement and discrimination strategies for nonorthogonal coherent states are essential in quantum and classical communications[2–5] and in many implementations of quantum information science[6,7–9], such as quantum repeaters[8] and quantum computation[7,10], as well as for quantum-enhanced metrology[11–13]. The nonorthogonal nature of these states is the basis for many of these applications, particularly those involving communication security[3,14–16]. Coherent states are ideal for communications; they are easy to prepare and manipulate, they are resilient to losses and can maximize the information transmitted in the communication channel[17], and allow for communications over long distances[18]. The use of multiple coherent states to encode information, for example in the phase of the field using phase-shift keying (PSK), can increase the spectral efficiency of the communication channel[5,18], and may increase the secret key rate in quantum key distribution[19,20] in extended communication links[21].

The performance of quantum information and communication protocols using coherent states can be maximized with optimized strategies for the detection and discrimination of these states. The standard quantum limit (SQL) defines the minimum error with which nonorthogonal states can be distinguished by direct measurement of the physical property of the light used to encode the information, such as intensity or phase. This minimum error is what ideal, 100% efficient, conventional receivers can achieve[22]. Remarkably, quantum mechanics allows for a lower error bound, known as the Helstrom bound[1], which can be approached or achieved by optimized discrimination strategies. Identifying physically realizable techniques for implementing such strategies has been and remains a major technical challenge.

Implementations of quantum receivers using optimized strategies to discriminate two non-orthogonal coherent states have been extensively investigated[23–30]. Recently, a quantum receiver using a near-unity efficiency detector for the first time demonstrated the discrimination of two nonorthogonal states below the SQL (for a small range of optical power and with error probabilities 0.2 dB below the SQL)[31]. In general, the discrimination of multiple (more than 2) nonorthogonal coherent states below the SQL[1] is achievable using optimized strategies to test multiple hypotheses for the incident state[32–37]. Experimental investigations using post-processing have shown the potential of some of these strategies[34,35] to discriminate multiple nonorthogonal states below the SQL. A recent work demonstrated a receiver demodulating 4 pulse-position-modulation encoded coherent states and observed lowered error probabilities when compared with direct detection under the same experimental conditions (i.e., a direct detector with the same efficiency as the receiver)[38]. However, there have been no unconditional demonstrations (that is as compared to 100% efficient detection) of discrimination of multiple nonorthogonal states below the SQL.

We present the first demonstration of a quantum receiver that unconditionally discriminates among four nonorthogonal coherent states in a quadrature PSK format (QPSK) as shown in Fig. 1a with error probabilities as low as one fourth of the SQL. We use a strategy for M-ary PSK states[34] based on photon counting and adaptive measurements[11,12,29,39,40] in the

form of fast feedback. This scheme can achieve low error probabilities using very few adaptive measurements and practical detection efficiencies[34]. We implement this strategy using a receiver with high bandwidth and high detection efficiency to obtain error rates four times lower than the theoretical limit of a perfect 100% efficient conventional coherent receiver (i.e. the SQL). In addition, this quantum receiver unconditionally surpasses the SQL for a wide range of powers of the input state.

Feedback State Discrimination

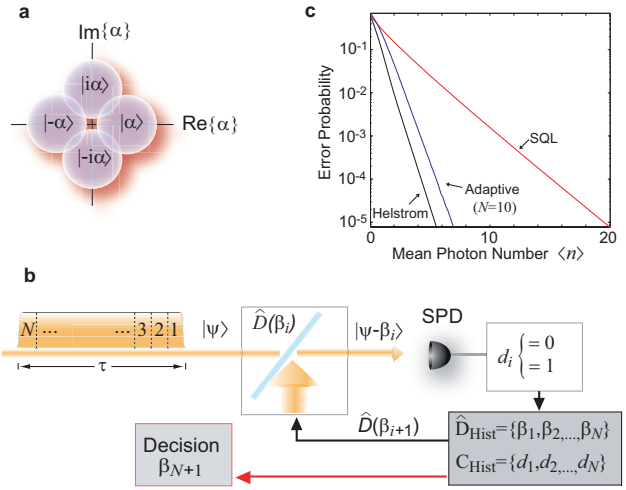

FIG. 1: **Discrimination strategy**. **a**, Nonorthogonal coherent states in the QPSK format: $\{|\alpha\rangle,\ |i\alpha\rangle, |-\alpha\rangle, |-i\alpha\rangle\}$. **b**, Adaptive-measurement discrimination strategy based on N adaptive measurements, updated optical displacements $\hat{D}(\beta_i)$ and photon counting d_i (see text for details.) **c**, Error probabilities for the discrimination of QPSK states for the strategy with 10 adaptive measurements (blue) are below the SQL (red) and approach the Helstrom bound (black).

Figure 1b shows the measurement approach for multiple nonorthogonal state discrimination, which consists of N consecutive adaptive measurements with equal duration (feedback periods) of the input field $|\psi\rangle$ in the form of feedback. In each adaptive measurement j ($j = 1, 2, 3, ..., N$), the strategy tests the hypothesized state $|\beta_j\rangle$, which corresponds to the most probable state of the input field $|\psi\rangle$; it performs a displacement $\hat{D}(\beta_j)$ of $|\psi\rangle$ to $|\psi - \beta_j\rangle$; and detects the number of photons d_j of the displaced field using a single-photon detector (SPD). If the hypothesis is correct, then $|\beta_j\rangle = |\psi\rangle$, the input field is displaced to vacuum during this feedback period and the number of detected photons d_j is always zero. After this measurement, the strategy estimates the new most probable state $|\beta_{j+1}\rangle$ to be tested in the subsequent feedback period using Bayesian inference based on the detection history $C_{\rm Hist}$ and displacement history $\hat{D}_{\rm Hist}$. The new most probable state corresponds to the one with the maximum of the posterior probabilities

$$\boldsymbol{P}_{\rm post}(\{|\psi\rangle\}|\beta_j, d_j) = A\ \mathbb{P}(d_j|\beta_j, \{|\psi\rangle\})\ \boldsymbol{P}_{\rm prior}(\{|\psi\rangle\}), \quad (1)$$

where $\boldsymbol{P}_{\rm post}\ (\{|\psi\rangle\}|\beta_j, d_j)$ and $\boldsymbol{P}_{\rm prior}(\{|\psi\rangle\})$ are the posterior and prior probabilities, respectively, for all possible input states $\{|\psi\rangle\}$, $\mathbb{P}(d_j|\beta_j, \{|\psi\rangle\})$ are conditional Poissonian probabilities of observing the detection result d_j for $\{|\psi\rangle\}$ given the displacement field β_j, and A is the normalization factor obtained from summing Eq. (1) over all the possible states $\{|\psi\rangle\}$. In each subsequent feedback period, the Bayesian probabilities are updated so that $\boldsymbol{P}_{\rm post}$ of period j becomes $\boldsymbol{P}_{\rm prior}$ in period $j+1$. The final determination of the state of the input field $|\psi\rangle$ corresponds to the most probable state $|\beta_{N+1}\rangle$ determined in the last adaptive measurement N[34]. The probability of error associated with identifying the input state decreases with higher numbers of adaptive measurements, surpassing the SQL to a higher degree and approaching the Helstrom bound[34]. Fig. 1c shows the error probability for the discrimination of the four nonorthogonal coherent states shown in Fig. 1a using this strategy with 10 adaptive measurements, together with the SQL given by

$$P_{\rm SQL} = 1 - [1 - \frac{1}{2}{\rm erfc}(\sqrt{|\alpha|^2/2})]^2, \quad (2)$$

where ${\rm erfc}(x) = \frac{2}{\sqrt{\pi}}\int_x^\infty e^{-t^2}dt$, and the Helstrom bound for this case[1]. We implement this strategy with a system with high detection efficiency and high bandwidth to discriminate these states below the SQL.

Experimental Implementation

Figure 2 shows the experimental realization of the quantum receiver for the unconditional discrimination of multiple nonorthogonal states. A frequency- and power-stabilized laser at 633 nm together with an acousto-optic modulator (AOM) and a single-mode fibre (SMF) prepare flat-top light pulses in a coherent state of duration 27 μs at a rate of 12.5 kHz. The light pulses enter into a Mach-Zehnder interferometer where a 50/50 beam splitter (BS_1) splits the light into two optical paths. Light pulses in the upper path are attenuated by a factor of 100, and fed into a fibre-based phase modulator (PM_1) which prepares the quantum state to be discriminated $|\psi\rangle \in \{|\alpha\rangle,\ |i\alpha\rangle, |-\alpha\rangle, |-i\alpha\rangle\}$. A second phase modulator (PM_2) in the lower path prepares the strong field to perform the displacement of the input field $|\psi\rangle$ in a 99:1beam splitter (BS_2) which transmits 99% of $|\psi\rangle$ and 1% of the strong displacement field. At the output of this beam splitter, these fields have strengths matched to within 0.1%, so that opposite relative phases accurately displace the input state to the vacuum. A SPD avalanche photodiode with measured detection efficiency of 84.0(5)% (See Methods for details about the SPD and associated uncertainties) at 633 nm and 10 dark counts per second detects the photons in the displaced field and a field-programmable gate array (FPGA) collects these detection events. The FPGA prepares the input state $|\psi\rangle$ and the displacement field independently using two 4-input fast multiplexers that provide controllable voltages to PM_1 and PM_2. Using the strategy above, the

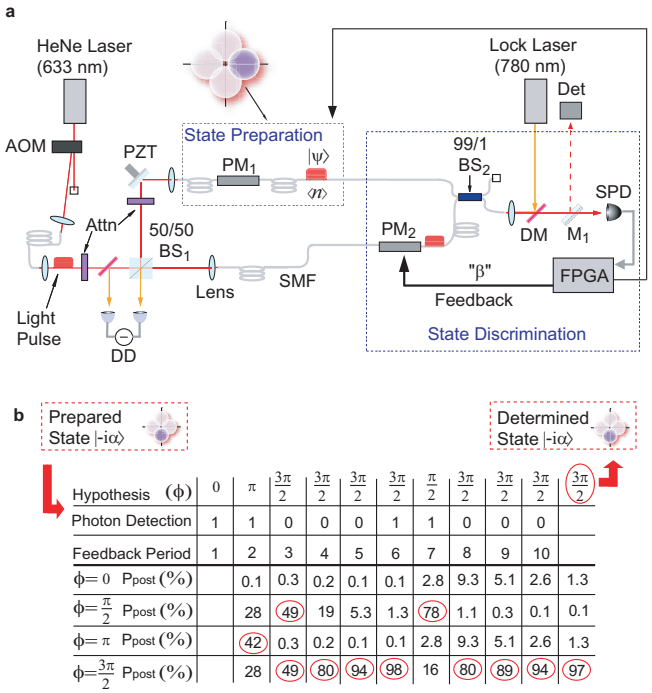

Hypothesis (ϕ)	0	π	$\frac{3\pi}{2}$	$\frac{3\pi}{2}$	$\frac{3\pi}{2}$	$\frac{3\pi}{2}$	$\frac{\pi}{2}$	$\frac{3\pi}{2}$	$\frac{3\pi}{2}$	$\frac{3\pi}{2}$	$\frac{3\pi}{2}$
Photon Detection	1	1	0	0	0	1	1	0	0	0	
Feedback Period	1	2	3	4	5	6	7	8	9	10	
$\phi=0$ P_{post} (%)		0.1	0.3	0.2	0.1	0.1	2.8	9.3	5.1	2.6	1.3
$\phi=\frac{\pi}{2}$ P_{post} (%)		28	49	19	5.3	1.3	78	1.1	0.3	0.1	0.1
$\phi=\pi$ P_{post} (%)		42	0.3	0.2	0.1	0.1	2.8	9.3	5.1	2.6	1.3
$\phi=\frac{3\pi}{2}$ P_{post} (%)		28	49	80	94	98	16	80	89	94	97

FIG. 2: **Experimental implementation of the quantum receiver. a**, The phase modulator PM_1, along with the set of attenuators Attn, prepare the state of the input field $|\psi\rangle$ to be discriminated in a light pulse at 633 nm with a given mean photon number $\langle n\rangle$. It is from this point, as indicated by $|\psi\rangle$, that $\langle n\rangle$ is defined for the state. The determination of $\langle n\rangle$ for this point is made using a calibrated detector Det and mirror M_1 flipped into the beam path during the calibration. The receiver measures the state of the input field using adaptive displacements, prepared with the phase modulator PM_2 and performed in the beam splitter BS_2, and photon counting with the single photon detector SPD using fast ($\approx$ 120 ns) feedback. Active path-length stabilization of the interferometer is realized using a second laser at 780 nm, differential detection with a differential detector DD and the piezo-electric transducer PZT-mounted mirror (see text for details.) **b**, A sample experimental run of the adaptive-measurement discrimination of the input state $|-i\alpha\rangle$. In this case, the receiver's final decision about the input state after the last feedback period corresponds to a success. The circles indicate the maximum posterior probabilities, in percentage, for the input state determined from the previous measurements. In this sample, the hypothesis in feedback period 4, $\frac{3\pi}{2}$, is randomly chosen between $\frac{\pi}{2}$ and $\frac{3\pi}{2}$ since at this point these phases are equally likely with $P_{\rm Post} = 49\%$.

FPGA processes the detection data in real time, determines the most probable input state, and prepares new displacements for the subsequent adaptive measurements of the incoming field. The discrimination procedure consists of 10 feedback periods of about 2.7 μs each, with a feedback bandwidth of 10 MHz limited by the electronic and optical delays, which are due to the multiplexers and phase modulators response times, the input-output latency of the SPD, the FPGA processing time, and the propagation time of light from PM_2 to the SPD. During each feedback period, the receiver detects the presence or absence of photons, and at the end of each period it updates the displacement field for subsequent measurements independently of the arrival time of the photons. Asynchronous updating of the displacements as soon as a detection is made might improve the receiver's performance somewhat and might be considered in the future.

Proper performance of this receiver requires good phase stability between the two optical paths in the interferometer and calibration and control of the phases of the input and displacement fields. The phase of the interferometer is actively stabilized using light from a 0.1 mW continuous wave (CW) laser at 780 nm and frequency-stabilized to an atomic line of rubidium (see Fig. 2a). It propagates in the opposite direction with respect to the 633 nm light inside the interferometer using dichroic mirrors (DM) with high transmittance (reflectance) of light at 633 nm (780 nm). The insertion loss of the phase modulator PM_1, and similarly of PM_2, at 633 nm and 780 nm is less than 3.5 dB and 4.2 dB respectively. A differential detector (DD) measures the interference at 780 nm and provides an electronic signal to actively stabilize the interferometer by applying feedback to a piezo-electric transducer (PZT) on the back of a mirror. Fig. 3a shows the two interference patterns for the two lasers in CW mode as observed at opposite sides of the interferometer. We scan the phase using the PZT and observe a 633 nm fringe visibility of $\mathcal{V} = 99.7\%$. When the interferometer is actively stabilized, the observed phase noise is smaller than 10 mrad.

Fig. 3b shows the control sequence for the operation of the receiver and the phase calibration of the input and displacement fields. The Lock-On time of 42 μs is when the 780 nm Lock laser is monitored and the interferometer is actively stabilized. The Lock-Off time (also 42 μs) is used for two tasks. It is during this Lock-Off time that the 633 nm laser is pulsed on for use either to calibrate the phases of the input and displacement fields or to operate the adaptive receiver.

The phase calibration of the input state $|\psi\rangle$ and displacement fields is done by observing the interference at the output of BS_2 as we apply different phase shifts to the 633 nm light pulses with PM_1 and PM_2. Fig. 3b shows the interference of 633 nm pulses when PM_1 prepares each of the states $\{|\alpha\rangle,\ |i\alpha\rangle, |-\alpha\rangle, |-i\alpha\rangle\}$. The estimated phase error of this calibration is below 10 mrad. We calibrate the phases of the displacement field by displacing to vacuum the state prepared with these particular phases as shown by the black line in Fig. 3b. The observed maximum-to-minimum signal ratio in the pulse-mode operation is $1.3(3)\times10^{-3}$ corresponding to a visibility of $\mathcal{V}_{\rm pulse}$=99.75(7)%, which is consistent with the visibility observed in the CW mode operation. This high visibility is achieved with precise control of the relative polarization between the two optical fields inside the interferometer together with good temporal and spatial overlap, while active temperature stabilization of PM_1

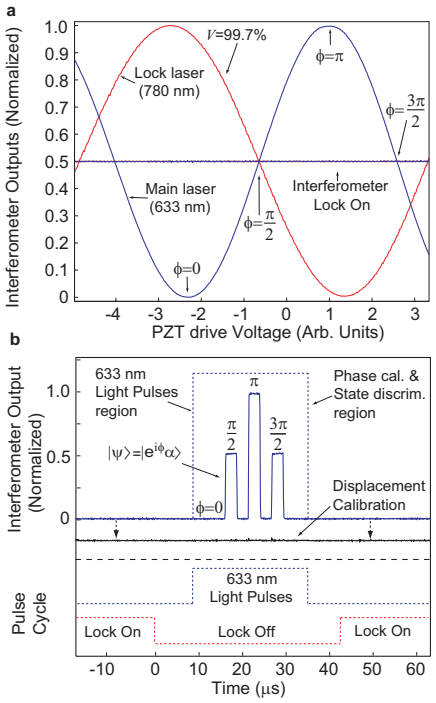

FIG. 3: **Phase measurement and preparation**. **a**, Interference fringes of CW light at 633 nm (blue line) and 780 nm (red line) as seen at opposite ends of the interferometer. The phases used to prepare the input states $\{|\alpha\rangle,\ |i\alpha\rangle, |-\alpha\rangle, |-i\alpha\rangle\}$ are indicated as $\{0,\ \pi/2,\ \pi, 3\pi/2\}$ respectively. The blue line at a level of 0.5 shows the light level at 633 nm when the interferometer is stabilized at $\phi = \pi/2$. **b**, Control sequence for calibration and phase preparation of the input state $|\psi\rangle$ and displacement fields using light pulses of 27 μs at 633 nm during the Lock-Off period of the interferometer stabilization cycle as indicated in the lower section of the figure. For illustration purposes, a waveform (blue line) shows the interference at 633 nm when PM_1 prepares the four possible phases $\phi = \{0,\ \pi/2,\ \pi, 3\pi/2\}$ for the input state $|\psi\rangle = |e^{i\phi}\alpha\rangle$. Setting the phase to each of these values allows for calibration of the input state. For a state discrimination measurement ϕ would be constant for the duration of the Light-Pulses region. A signal level of 0 corresponds to the state preparation with $\phi = 0$. To calibrate the displacement field, a zero level is measured (solid black line shown shifted down for a better view). PM_2 prepares the phase of this field to obtain total destructive interference, i.e. displacement to vacuum, for every prepared state $\{|\alpha\rangle,\ |i\alpha\rangle, |-\alpha\rangle, |-i\alpha\rangle\}$.

and PM_2 ensures good phase stability.

The overall operational procedure for the experiment consists of: a) calibrate the input field and displacement field phases, b) set the mean photon number of the input field, and c) run the 10-adaptive-measurement strategy 10^6 times. This process is repeated for each new input field mean photon number.

Experimental Results

In the experiment, the FPGA implements the discrimination strategy accounting for the actual experimental parameters: the receiver's total detection efficiency $DE_{\rm Tot}$=72% (see Methods) and the observed visibility $\mathcal{V}$ = 99.7%. This strategy provides a more accurate description of the receiver and improves the discrimination process[34,41]. The FPGA transfers to a computer for further analysis the information about the input state, detection and displacement histories, and the final estimate of the state. Figure 2b shows a sample of the experimental data when the quantum receiver discriminates an incoming state prepared in $|-i\alpha\rangle$ with a mean photon number of $\langle n\rangle$ =5. After the last adaptive measurement, the most probable state determined by the receiver is the final estimate of the input state that, in this case, corresponds to a success.

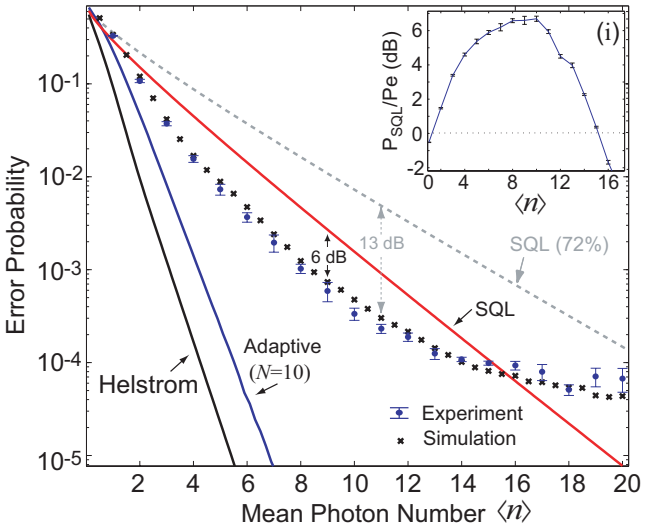

FIG. 4: **Experimental error probability.** The experimental error probability (blue dots) for the discrimination of 4 nonorthogonal states in the QPSK format together with the SQL (red line), SQL adjusted for the 72% detection efficiency of our receiver (dashed line), error probability limit for the optimized strategy with 10 adaptive measurements (blue line), and the Helstrom bound (black line). The experimental quantum receiver discriminates these states with lower error probabilities than the SQL for a range of mean-photon numbers from 2 to 15. Monte Carlo simulations (black crosses) of the strategy with $DE_{\rm Tot}$=72% and $\mathcal{V}$ = 99.7% show good agreement with the experimental observations. The inset (i) shows the experimental error probabilities (P_e) surpassing the SQL (P_{SQL}) by 6 dB from 6 to 11 mean photon numbers. This corresponds to achieving an error rate 4 times lower than the SQL. The error bars are 1-σ statistical uncertainties.

Figure 4 shows the experimental error probability in discriminating among four nonorthogonal coherent states in the QPSK format as a function of mean photon number $\langle n\rangle$ along with the SQL from Eq. (2), the SQL scaled to $DE_{\rm Tot}$=72%, the ideal limit for the optimized strategy with 10 adaptive measurements, and the Helstrom Bound. Each data point is the result of four sets of 10^6 independent experiments. The error bars are 1-σ statistical uncertainties, and the mean-photon

number uncertainty is 2% as described in the Methods. This quantum receiver discriminates four nonorthogonal coherent states below the SQL for mean photon numbers from 2 to 15 without any correction for detection inefficiencies. A higher number of adaptive measurements can result in lower error probabilities[34], but would require shorter delays necessary to prepare for subsequent adaptive measurements. We study the expected performance of the receiver for different detection efficiencies and visibilities. The theoretical predictions in Fig. 4 are based on Monte Carlo simulations of the strategy with 10 adaptive measurements and with the experimental parameters for detection efficiency DE_{Tot}=72% and visibility $\mathcal{V}$ = 99.7%. We do not observe any noticeable effect when we include the observed dark counts in the Monte Carlo simulations for the experimental input mean-photon numbers. We observe an excellent agreement between the experimental observations and these theoretical predictions. The upward curvature seen in the simulation and the experimental data as the mean photon number increases is due to less than 100% visibility which degrades the performance of the receiver for higher mean photon numbers. Less than 100% detection efficiency results in an overall shallower slope than the ideal result of Fig. 1c. The measured error probability beats the SQL by more than 6 dB for mean photon numbers from 6 to 11 as shown in the inset (i). These experimental results demonstrate the unconditional discrimination of multiple nonorthogonal states below the SQL.

Conclusion

Quantum adaptive measurements are an essential resource for many quantum information science applications; they allow us to perform tasks that are otherwise fundamentally impossible relying on conventional technologies. We have demonstrated a quantum receiver implementing adaptive displacement operations and photon-counting that unconditionally discriminates four nonorthogonal coherent states in a QPSK format significantly below the SQL for a wide range of optical powers. This receiver uses a strategy that can surpass the SQL with very few adaptive measurements and practical detection efficiencies. The receiver exploits its high bandwidth and high detection efficiency to achieve error rates four times lower than any ideal conventional receiver, and it can be extended to higher modulation formats. While we implemented the strategy in a feedback mode for convenience, it could be implemented in a feed-forward manner allowing much higher throughputs. This quantum receiver can be used to optimize future implementations of protocols in quantum information science, increase quantum communication rates over long distances, and potentially enable high-spectral bandwidth communications below the SQL.

Methods

Calibration of the SPD, mean-photon number and system detection efficiency. Our SPD is a commercial avalanche photodiode[43] whose detection efficiency we calibrated using a photodiode-based light-trapping detector that has a 0.05% uncertainty tied to an absolute spectral response scale at NIST[42](Note that all uncertainties of measurements made using this trap detector are 1- σ combined standard deviations). This photodiode trap was also used to calibrate a series of attenuators used to step down the output of a power-stabilized 633 nm laser allowing calibrated measurements at single-photon-levels. Thus we determined the SPD's detection efficiency to be 84.0(5)%. We applied the same methodology to calibrate the mean-photon number of the prepared input state in our experiment. We used another series of attenuators (after the first SMF and lens) to prepare the input light at the single-photon level with a 1- σ uncertainty of 1.7%. In addition, we calibrate the total transmittance of the optical components (T_1=92.5(2)%) from the point where the state is prepared to where its absolute power is measured by detector Det as shown in Fig. 2a. This results in a total uncertainty for the calibration of the absolute average photon number per pulse of $\sigma_{\langle n\rangle}$=2%. The receiver's expected total detection efficiency DE_{Tot}=72.3(7)% is obtained from the product of transmittance T_1, the SPD detection efficiency DE_{SPD}=84.0(5)%, transmittance T_2=97.0(5)% of the optical components before the SPD, and bandwidth-related losses (loss≈4%). The bandwidth-related losses are calculated from the fraction of time when the SPD output is ignored to avoid detecting events from previous feedback periods, due to finite bandwidth of the experiment.

*Certain commercial equipment, instruments or materials are identified in this paper to foster understanding. Such identification does not imply recommendation or endorsement by the National Institute of Standards and Technology, nor does it imply that the materials or equipment identified are necessarily the best available for the purpose.

Acknowledgements

F.E.B. thanks Sergey Polyakov and Alessandro Restelli for fruitful discussions about FPGA programming and low-noise electronic design, respectively, and thanks Ian Spielman for providing the laser diode at 780 nm.

Author Contributions

F.E.B. designed the experimental implementation of the receiver, performed the measurements and analyzed the experimental results. J.F. and A.M. provided assistance. J.G., J.K. and G.B. conceived the initial theoretical measurement strategy. All authors contributed to writing the manuscript.

Author Information

The authors declare no competing financial interests. Reprints and permissions of information are available at www.nature.com/reprints. Correspondence and requests for materials should be addressed to F.E.B. (fbecerra@umd.edu).

[1] Helstrom, C. W. *Quantum detection and estimation theory, Mathematics in Science and Engineering* **123** (Academic Press, 1976).

[2] Caves, C. M. & Drummond, P. D. Quantum limits on bosonic communication rates. *Rev. Mod. Phys.* **66**, 481–537 (1994).

[3] Grosshans, F. & Grangier, P. Continuous variable quantum cryptography using coherent states. *Phys. Rev. Lett.* **88**, 057902 (2002).

[4] Grosshans, F. *et al.* Quantum key distribution using gaussian-modulated coherent states. *Nature* **421**, 238–241 (2003).

[5] S Betti, G. D. & ELannone. *Coherent optical communications systems* (Wiley, 2000).

[6] Weedbrook, C. *et al.* Gaussian quantum information. *Rev. Mod. Phys.* **84**, 621–669 (2012).

[7] Munro, W. J., Nemoto, K. & Spiller, T. P. Weak nonlinearities: a new route to optical quantum computation. *New J. Phys.* **7**, 137 (2005).

[8] van Loock, P. Optical hybrid approaches to quantum information. *Laser Photon. Rev.* **5**, 167–200 (2011).

[9] Nemoto, K. & Munro, W. J. Nearly deterministic linear optical controlled-not gate. *Phys. Rev. Lett.* **93**, 250502 (2004).

[10] Ralph, T. C., Gilchrist, A., Milburn, G. J., Munro, W. J. & Glancy, S. Quantum computation with optical coherent states. *Phys. Rev. A* **68**, 042319 (2003).

[11] Wiseman, H. M. Adaptive phase measurements of optical modes: Going beyond the marginal Q distribution. *Phys. Rev. Lett.* **75**, 4587–4590 (1995).

[12] Armen, M. A., Au, J. K., Stockton, J. K., Doherty, A. C. & Mabuchi, H. Adaptive homodyne measurement of optical phase. *Phys. Rev. Lett.* **89**, 133602.

[13] Wiseman, H. & Milburn, G. *Quantum Measurement and Control* (Cambrige University Press, 2010).

[14] Gisin, N., Ribordy, G., Tittel, W. & Zbinden, H. Quantum cryptography. *Rev. Mod. Phys.* **74**, 145–195 (2002).

[15] Bennett, C. H. Quantum cryptography using any two nonorthogonal states. *Phys. Rev. Lett.* **68**, 3121–3124 (1992).

[16] Huttner, B., Imoto, N., Gisin, N. & Mor, T. Quantum cryptography with coherent states. *Phys. Rev. A* **51**, 1863–1869 (1995).

[17] Giovannetti, V. *et al.* Classical capacity of the lossy bosonic channel: The exact solution. *Phys. Rev. Lett.* **92**, 027902 (2004).

[18] Agarwal, G. S. *Fiber-Optic Communication Systems* (Wiley, 2010).

[19] Weedbrook, C. *et al.* Quantum cryptography without switching. *Phys. Rev. Lett.* **93**, 170504 (2004).

[20] Sych, D. & Leuchs, G. Coherent state quantum key distribution with multi letter phase-shift keying. *New J. Phys.* **12**, 053019 (2010).

[21] Leverrier, A. & Grangier, P. Unconditional security proof of long-distance continuous-variable quantum key distribution with discrete modulation. *Phys. Rev. Lett.* **102**, 180504 (2009).

[22] Proakis, J. G. *Digital Communications, 4th Ed.* (McGraw-Hill, 2000).

[23] Kennedy, R. S. A near-optimum receiver for the binary coherent state quantum channel. MIT Res. Lab. Electron. Quart. Progr. Rep. **110**, 219-225 (1972).

[24] Dolinar, S. J. A optimum receiver for the binary coherent state quantum channel. MIT Res. Lab. Electron. Quart. Progr. Rep. **111**, 115-120 (1973).

[25] Dolinar, S. J. *A Class of Optical Receivers Using Optical Feedback*. Ph.D. thesis, Massachusetts Institute of Technology (1976).

[26] Sasaki, M. & Hirota, O. Optimum decision scheme with a unitary control process for binary quantum-state signals. *Phys. Rev. A* **54**, 2728–2736 (1996).

[27] Takeoka, M. & Sasaki, M. Discrimination of the binary coherent signal: Gaussian-operation limit and simple non-gaussian near-optimal receivers. *Phys. Rev. A* **78**, 022320 (2008).

[28] Wittmann, C. *et al.* Demonstration of near-optimal discrimination of optical coherent states. *Phys. Rev. Lett.* **101**, 210501 (2008).

[29] Cook, R. L., Martin, P. J. & Geremia, J. M. Optical coherent state discrimination using a closed-loop quantum measurement. *Nature* **446**, 774–777 (2007).

[30] Tsujino, K. *et al.* Sub-shot-noise-limit discrimination of on-off keyed coherent signals via a quantum receiver with a superconducting transition edge sensor. *Opt. Express* **18**, 8107–8114 (2010).

[31] Tsujino, K. *et al.* Quantum receiver beyond the standard quantum limit of coherent optical communication. *Phys. Rev. Lett.* **106**, 250503–250506 (2011).

[32] Dolinar, S. J. A near-optimum receiver structure for the detection of m-ary optical ppm signals. Telecommunication and Data Acquisition Report 42-72, December 1982 (Jet Propulsion Laboratory).

[33] Bondurant, R. S. Near-quantum optimum receivers for the phase-quadrature coherent-state channel. *Opt. Lett.* **18**, 1896–1898 (1993).

[34] Becerra, F. E. *et al.* m-ary-state phase-shift-keying discrimination below the homodyne limit. *Phys. Rev. A* **84**, 062324 (2011).

[35] Muller, C. *et al.* Qpsk coherent state discrimination via a hybrid receiver. *New J. Phys.* **14**, 083009 (2012).

[36] Izumi, S. *et al.* Displacement receiver for phase-shift-keyed coherent states. *Phys. Rev. A* **86**, 042328 (2012).

[37] Nair, R., Yen, B. J., Guha, S., Shapiro, J. H. & Pirandola, S. Symmetric m-ary phase discrimination using quantum-optical probe states. *Phys. Rev. A* **86**, 022306 (2012).

[38] Chen, J., Habif, J. L., Dutton, Z., Lazarus, R. & Guha, S. Optical codeword demodulation with error rates below the standard quantum limit using a conditional nulling receiver. *Nature Photon.* **6**, 374–379 (2012).

[39] Higgins, B. L., Berry, D. W., Bartlett, S. D., Wiseman, H. M. & Pryde, G. J. Entanglement-free heisenberg-limited phase estimation. *Nature* **450**, 393–396 (2007).

[40] Xiang, G. Y., Higgins, B. L., Berry, D. W., Wiseman, H. M. & Pryde, G. J. Entanglement-enhanced measurement of a completely unknown optical phase. *Nature Photon.* **5**, 43–47 (2011).

[41] Zhang, L. *et al.* Mapping coherence in measurement via full quantum tomography of a hybrid optical detector. *Nature Photon.* **6**, 364–368 (2012).

[42] Gentile, T. R., Houston, J. M. & Cromer, C. L. Realization of a scale of absolute spectral response using the national institute of standards and technology high-accuracy cryo-

genic radiometer. *Appl. Opt.* **35**, 4392–4403 (1996).
[43] PicoQuant, model Tau-SPAD-100**.